March 1991

UILU-ENG-91-2213
DC-128

(2)

Decision and Control Laboratory

AD-A232 890

AUTOMATED ARC WELDING SYSTEM

James Hugh Ross

Coordinated Science Laboratory
College of Engineering
UNIVERSITY OF ILLINOIS AT URBANA-CHAMPAIGN

UNCLASSIFIED

SECURITY CLASSIFICATION OF THIS PAGE

REPORT DOCUMENTATION PAGE

Form Approved OMB No. 0704-0188

1a. REPORT SECURITY CLASSIFICATION Unclassified	1b. RESTRICTIVE MARKINGS None
2a. SECURITY CLASSIFICATION AUTHORITY	3. DISTRIBUTION/AVAILABILITY OF REPORT Approved for public release; distribution unlimited
2b. DECLASSIFICATION/DOWNGRADING SCHEDULE	
4. PERFORMING ORGANIZATION REPORT NUMBER(S) UILU-ENG-91-2213 (DC-128)	5. MONITORING ORGANIZATION REPORT NUMBER(S)
6a. NAME OF PERFORMING ORGANIZATION Coordinated Science Lab University of Illinois 6b. OFFICE SYMBOL (If applicable) N/A	7a. NAME OF MONITORING ORGANIZATION US Army Construction Research Laboratory
6c. ADDRESS (City, State, and ZIP Code) 1101 W. Springfield Ave. Urbana, IL 61801	7b. ADDRESS (City, State, and ZIP Code) P. O. Box 4005 Champaign, IL 61824-4005
8a. NAME OF FUNDING/SPONSORING ORGANIZATION US Army Construction Res. Lab 8b. OFFICE SYMBOL (If applicable)	9. PROCUREMENT INSTRUMENT IDENTIFICATION NUMBER DACA 88-90-D-0003-14
8c. ADDRESS (City, State, and ZIP Code) P. O. Box 4005 Champaign, IL 61824-4005	10. SOURCE OF FUNDING NUMBERS PROGRAM ELEMENT NO. / PROJECT NO. / TASK NO. / WORK UNIT ACCESSION NO.
11. TITLE (Include Security Classification) AUTOMATED ARC WELDING SYSTEM	
12. PERSONAL AUTHOR(S) ROSS, JAMES HUGH	
13a. TYPE OF REPORT Technical 13b. TIME COVERED FROM _____ TO _____	14. DATE OF REPORT (Year, Month, Day) 1991 March 15. PAGE COUNT 42
16. SUPPLEMENTARY NOTATION	

17. COSATI CODES			18. SUBJECT TERMS (Continue on reverse if necessary and identify by block number)
FIELD	GROUP	SUB-GROUP	Arc welding, puddle geometry, linear quadratic control, control system hierarchy.

19. ABSTRACT (Continue on reverse if necessary and identify by block number)

An experimental automated arc welding system is presented. A general overview of the system capabilities is given. This is followed by a more detailed description of the new measurement techniques which have been incorporated. A description of the control system structure includes details of some implementation considerations. This is followed by an example of a controller which has been implemented. Finally, suggestions for further research are presented.

20. DISTRIBUTION/AVAILABILITY OF ABSTRACT ☒ UNCLASSIFIED/UNLIMITED ☐ SAME AS RPT. ☐ DTIC USERS	21. ABSTRACT SECURITY CLASSIFICATION Unclassified
22a. NAME OF RESPONSIBLE INDIVIDUAL	22b. TELEPHONE (Include Area Code) / 22c. OFFICE SYMBOL

DD Form 1473, JUN 86 Previous editions are obsolete. SECURITY CLASSIFICATION OF THIS PAGE

UNCLASSIFIED

ABSTRACT

An experimental automated arc welding system is presented. A general overview of the system capabilities is given. This is followed by a more detailed description of the new measurement techniques which have been incorporated. A description of the control system structure includes details of some implementation considerations. This is followed by an example of a controller which has been implemented. Finally, suggestions for further research are presented.

AUTOMATED ARC WELDING SYSTEM

BY

JAMES HUGH ROSS

B.S., University of Illinois, 1989

THESIS

Submitted in partial fulfillment of the requirements
for the degree of Master of Science in Electrical Engineering
in the Graduate College of the
University of Illinois at Urbana-Champaign, 1991

Urbana, Illinois

ACKNOWLEDGMENTS

This research was supported by the US Army Construction Engineering Research Laboratory (USACERL). This thesis contains a description of a complex system which has been under development for many years. Over the years, many people have contributed to it in many ways. It would be impossible to list the names of all of these people. I wish to specifically thank Professor Petar Kokotovic and Mr. Robert Weber for their guidance and support, Jeff Schiano and Dan Henderson for making the many hours of work more fun, and Thierry Bourret, Lake Lattimore and Will Windes for their assistance. Finally, I would like to thank my parents for their support and advice during my seemingly never-ending college career.

TABLE OF CONTENTS

CHAPTER 1

INTRODUCTION

1.1 Background

Welding is a complex process that depends on a number of parameters. Factors such as the thermal properties of the material used, the initial temperature of the material, the presence of heat sinks on or near the weld path and the physical geometry of the joint can all affect the quality of a weld joint [1]. Many parameters vary during the weld process which may lead to weld defects. Since the dominant cost factors in welding are labor and the expense of locating and repairing defects, there has been a strong effort to design automated welding systems which produce consistently good welds despite variations in material parameters and other disturbances. Although there has also been an effort to develop a system which will track a desired trajectory while welding, this problem is not addressed here. Instead, this research has focused on developing methods of improving the quality of the automated weld. To date, the application of this research has been limited to long straight welds.

The gas metal arc welding (GMAW) process joins materials through the coalescence of a consumable metal electrode and the workpiece. A wire feed mechanism continually draws electrode wire from a spool and pushes it through the electrode assembly. The electrode wire is held at a positive potential above the workpiece causing an electric arc to be sustained between the electrode tip and the workpiece. Droplets of metal ejected from the electrode tip convey heat to the workpiece and form a puddle directly beneath the arc comprised of electrode and workpiece metal. The puddle solidifies to form the weld joint as the electrode assembly is moved across the workpiece. During the welding

process the region near the arc is purged with an inert gas mixture to avoid contamination and oxidation of the weld joint. In conventional GMAW, the controlled inputs are the arc current and the travel rate of the electrode.

The shape of the molten weld puddle plays an important role in determining the integrity of the weld joint [1]-[3]. For this reason, several researchers have developed methods for measuring [4]-[8] and regulating [4],[8]-[15] puddle geometry. Many of these studies employ PI or PID control designs with very little effort given to modeling the dynamics of the weld process.

1.2 System Description

A facility for developing and evaluating an automated welding system has been developed at USACERL in conjunction with the University of Illinois. The system consists of a gas metal-arc welding (GMAW) torch, two cameras, two computers, and a number of various sensors. The cameras capture images of the welding process which are processed by one computer to measure some of the more important process parameters. The second computer implements the control algorithms and stores data for later analysis.

An image processing system supported by a dedicated computer obtains measurements of the puddle geometry at discrete time instants [8], [16]. Puddle images are obtained from a CCD camera attached to the torch holder. The image processing system can acquire an image and estimate the puddle geometry in about 50 ms. A second computer system implements control loops and supervises the image processing computer. Figure 1.1 shows the computers and other hardware used for both measurement and control purposes. The figures appear at the end of the chapters. Starting in the upper-right-hand corner, the two monitors display the images captured by the cameras. Below these are the image processing computer and a VCR which records images from the cameras. On the left-hand side is the computer which implements the control algorithms. Above this computer are various circuit boards which contain amplifiers, a clock circuit, relays and interfaces between the computers and the rest of the system.

Finally, the upper-left-hand side shows the Vanzetti optical pyrometer which measures bead temperature.

Figure 1.2 shows the welding torch, table and many of the sensors and actuators of the system. At the top right of the picture is a large spool of wire used during the weld process. The plate to be welded is mounted on the table using six brackets to keep it from bending from the large stresses caused by the welding process. The welding torch is located near the middle of the plate. The wirefeed assembly is located directly above the torch. The motor used to feed the wire and the tachometer used to determine the wirefeed rate are just above the torch. Above the motor is an encoder used to measure the amount of wire consumed. Figure 1.3 is a close-up of the torch assembly. The puddle geometry camera is directly to the left of the torch. Farther to the left is an optical sensor to measure the concentration of various gases within the arc plasma. The bead temperature camera and the optical sensor for the Vanzetti are located behind the torch. They are barely visible in this picture. The hose located to the right of the torch is used to carry the shield gas. The large duct located just above and to the right of the torch is used to carry the smoke and fumes away from the arc in order to give the cameras a clear view.

1.3 Outline

This thesis is basically a description of the GMAW system. Chapter 2 describes the measurement system and the image processing system. Chapter 3 describes the control system structure and implementation. Chapter 4 gives a description of a control algorithm which has been implemented on the system. Chapter 5 concludes with suggestions for further research.

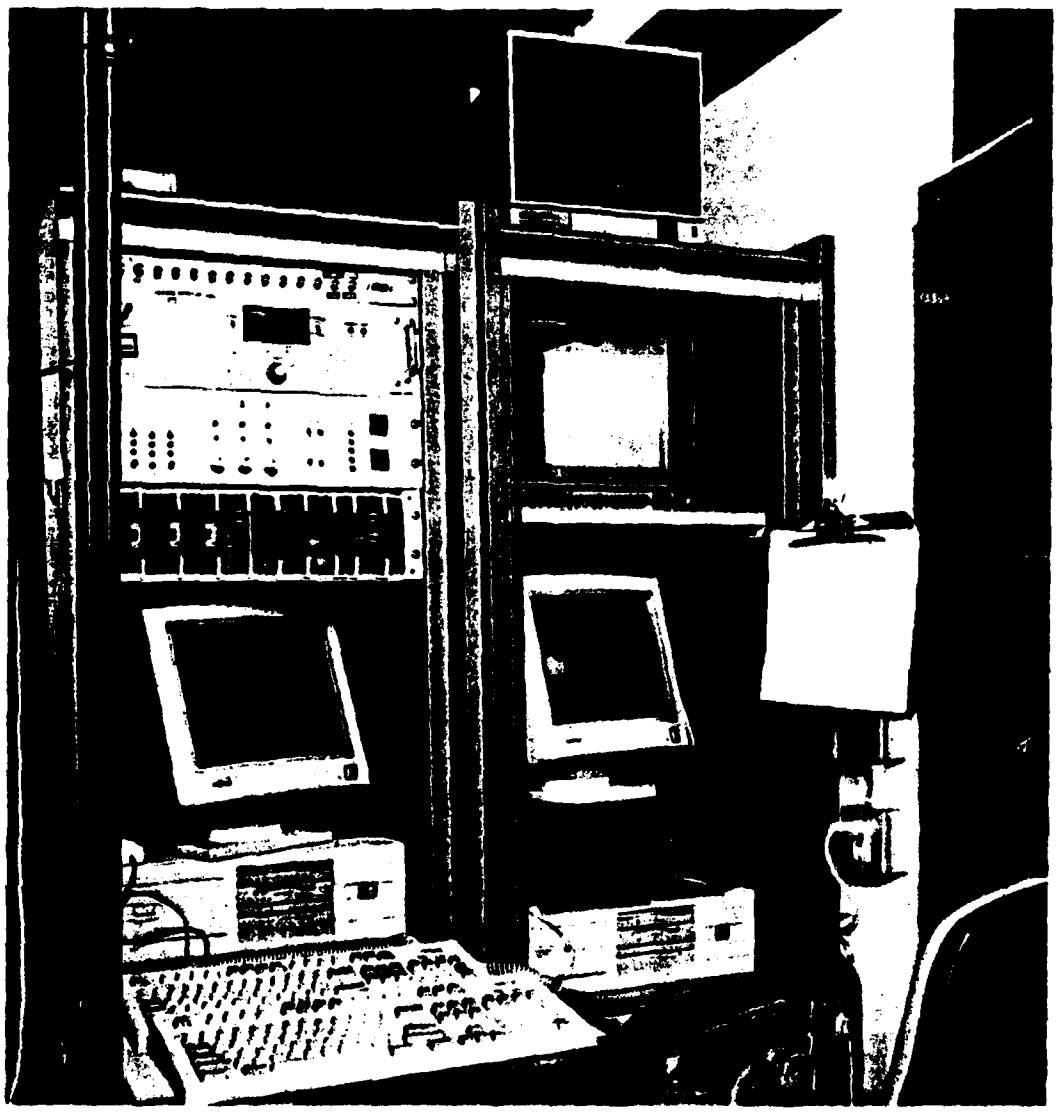

Figure 1.1: Computer system and associated hardware.

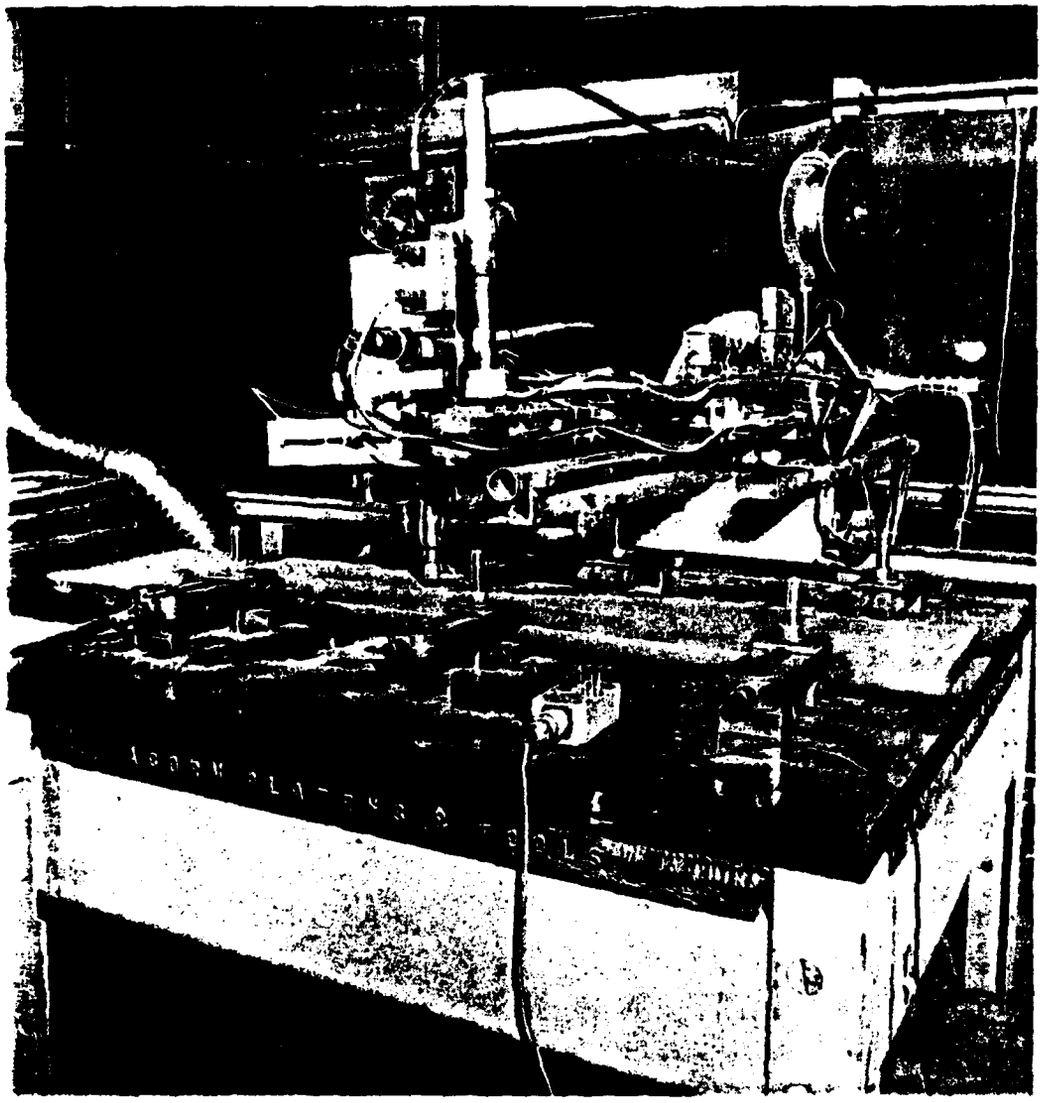

Figure 1.2: GMAW hardware.

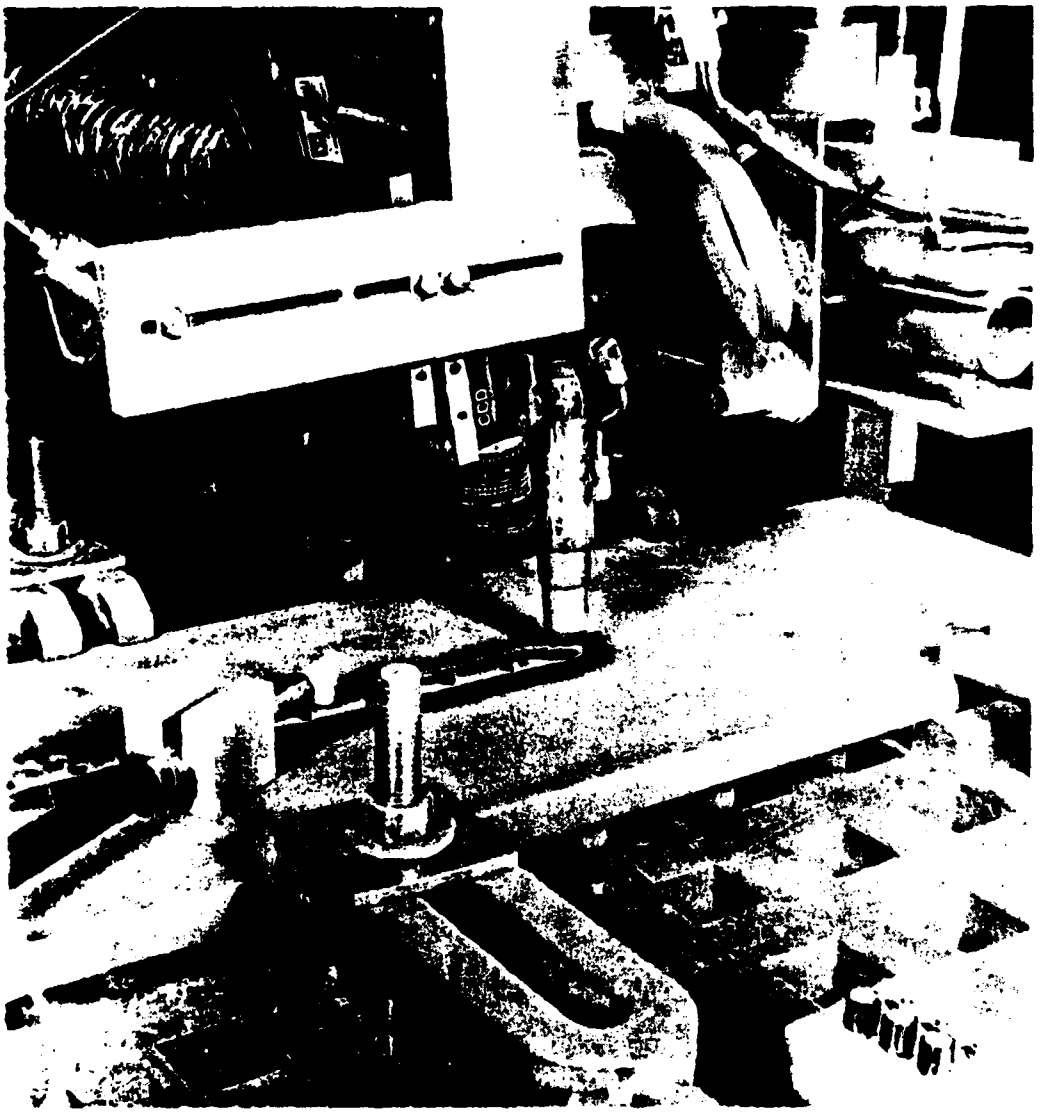

Figure 1.3: Close-up of torch assembly.

CHAPTER 2

MEASURING SYSTEM VARIABLES

2.1 Methods of Measuring Data

In order to control the weld process, reliable and accurate measurements of the process must be made. The variables which must be measured include travel rate, arc current, wirefeed rate, bead temperature, bead cooling rate, puddle width and puddle area. Standard measurement techniques allow measurement of travel rate, arc current, wirefeed rate and even bead temperature. However, measuring the bead cooling rate and puddle geometry is not as straightforward.

2.2 Standard Sensors

The travel rate and wirefeed rate can be measured using tachometers. A Hall sensor is used to measure arc current, and an optical pyrometer is used to measure bead temperature. These measurements, along with various motor currents, voltages and thermocouple readings, are read directly into the control computer after passing through a set of voltage followers used to isolate the computer from the weld process. The analog to digital (A/D) conversion results in a set of integers representing the current values of each measured variable. These integers are converted to real numbers using a set of conversion constants. Each data variable has its own set of conversion constants which convert the integer value to a real number which has the appropriate engineering units. For example, a D/A reading of 200 might represent a travel rate of 16.01 inches per minute (IPM) or a puddle width of 0.391". Since most of the data must pass through

either an A/D converter or a D/A converter, it is convenient to have both integer and real number forms of each variable. This also enables the data to be stored efficiently in a file of integers for later analysis.

2.3 The Image Processing System

Measuring bead cooling rate and weld puddle geometry is accomplished through the use of a dedicated image processing system. This system consists of two Sony CCD cameras mounted behind the welding torch. One camera looks down at the tail end of the liquid weld puddle, while the other camera focuses on the solidified weld bead approximately 2″ to 5″ behind the torch. The images from these cameras are processed by a Compaq 386/33 computer equipped with two DataCube AT-428 Image Processing Boards. This computer processes both images and calculates the puddle width, puddle area and spatial temperature gradient every 240 ms. These data are then fed to another Compaq 386/33 computer which implements the control algorithms and collects data for later analysis.

2.4 Measuring Cooling Rate

Two common methods are often used to measure or estimate cooling rate. The usual method of measuring cooling rate involves using infrared cameras which give accurate results but are cost prohibitive. The usual method of estimating the cooling rate involves making the assumption that the inputs have been constant and that the system is in a quasi-steady-state condition. However, since this is a closed-loop system, the quasi-steady-state assumption is not valid. This makes it desirable to come up with a more direct measurement technique. The following algorithm, proposed by Schiano, uses a direct temperature measurement, a pixel intensity gradient, and the measured travel speed to calculate the cooling rate [20]. If these measurements are available, the cooling rate is given by

$$CR = \frac{dT}{dt} - \frac{dT}{dx}\frac{dx}{dt} \tag{2.1}$$

where

$$\frac{dT}{dt} = \textit{derivative of temperature measurement}$$
$$\frac{dT}{dx} = \textit{spatial gradient of temperature}$$
$$\frac{dx}{dt} = \textit{travel rate}$$

Since the temperature measurement is available every 40 ms from the optical pyrometer, a fairly accurate estimate of the derivative of the bead temperature can be determined. In order to reduce the noise associated with a derivative, an algorithm was developed which uses a number of previous samples to compute the derivative. This algorithm results in a smoother temperature derivative. The travel rate is a controlled variable and is measured every 40 ms. In order to measure cooling rate, it is necessary to measure the spatial gradient of the bead temperature distribution. This measurement is made by mapping pixel intensity to temperature. Figure 2.1 shows an image from the bead temperature camera. The small square shows the position on the bead which is used to determine temperature. This position is chosen to coincide with the measurement of the optical pyrometer. The average intensity of the pixels within the box can be mapped to temperature. The plate is assumed to act as a black body radiator. The map from intensity to temperature is a quartic map since intensity is known to vary with the fourth power of temperature for black body radiation. The map is calibrated to convert pixel intensity to °F. The map has proven to be quite accurate for a large part of the temperature range encountered when welding.

Figure 2.2 shows the same image with a larger box superimposed. This box outlines the region of the image used to determine the spatial temperature gradient, which is found by averaging the pixel intensities in the horizontal direction to reduce the effects of noise. These average intensities are found for each horizontal row of pixels in a vertical region centered around the desired measurement point. A least-square algorithm is used to estimate the pixel intensity gradient in units of Intensity/Pixel. This number is converted to units of °F/inch by mapping intensity to temperature and pixels to inches. The gradient information, combined with other measurements already available, allows

a dynamic measurement of cooling rate. This measurement of cooling rate compares favorably with an independent thermocouple measurement. The dynamic measurement was within 10% of the value of the cooling rate determined from the thermocouple data measured at three different operating points.

It is interesting from an engineering standpoint to note that this accurate measurement is relatively inexpensive. Most attempts to measure temperature and cooling rate involve infrared cameras, which can cost up to $40,000. The equipment used for this measurement totals less than $25,000 and provides both temperature and puddle geometry information.

2.5 Measuring Puddle Geometry

The measurement of the weld puddle geometry can be split into two distinct tasks. One task involves estimating the puddle width and area from puddle boundary data. The other task is to find the boundary data in the first place. This is not trivial. Difficulties in obtaining the boundary data result from problems such as arc noise as well as from tracking an image which changes in both size and location.

The shape of the weld puddle varies depending on the inputs. Both arc current and travel rate have effects on the width and area of the weld puddle. The weld puddle is usually shaped like a tear drop or an egg, but at times it can be elliptical or even circular. In order to estimate the puddle width and area, a mathematical model which accurately describes its shape must be found. This has proven to be rather difficult since the shape varies so drastically. Baheti chose to estimate the shape of the weld puddle as an ellipse [8]. This description has two advantages. First, an ellipse is a reasonable approximation to the weld puddle shape over a wide range of conditions. Second, the mathematical description of an ellipse is very simple. This fact greatly simplifies the numerical algorithms needed to estimate the puddle geometry. The major problem with using an ellipse to describe the weld puddle shape is that the weld puddle shape is not always elliptical.

The following algorithm is used to measure the puddle width and area. First, the image processing board captures an image of the liquid metal. Once the image is stored in memory, some of the pixels are used to determine the boundary points of the ellipse. The pixels used are those which lie on a number of search vectors, which are located normal to the boundary of the previously estimated ellipse. Figure 2.3 shows a picture of an image of a weld puddle with the set of search vectors superimposed on the image. The boundary point for each search vector is found by determining a threshold grey level value and finding the pixel along the search vector where this threshold value is exceeded. The threshold value is found by averaging the grey-level of three pixels from each end of the search vector. The grey level of each pixel along the search vector, starting from the outside, is compared to this threshold value. The first pixel whose grey level exceeds the threshold is the boundary point for that search vector. The boundary points for each search vector in Figure 2.3 are located at the boundary between black and white pixels along the search vectors. This figure shows that the algorithm used to find the boundary data works well.

Once all of the boundary points are determined, Baheti's algorithm is used to find a least-square estimate of the ellipse formed by the boundary points. The width and area of the ellipse are said to be the width and area of the weld puddle. Figure 2.4 shows the same image of the weld puddle with the estimated ellipse superimposed. The error in measurement is usually around 5% compared to the width and area found manually on a still image. Once the puddle geometry data have been found, a new set of search vectors is found. The new search vectors are normal to the boundary of the current ellipse and will be used to find the boundary data for the next image.

The method currently being used to measure width and area of the weld puddle is both accurate and robust. This is not by accident. Many revisions have been made to the algorithms to improve their performance. The historical development of the image processing system is given in the Appendix.

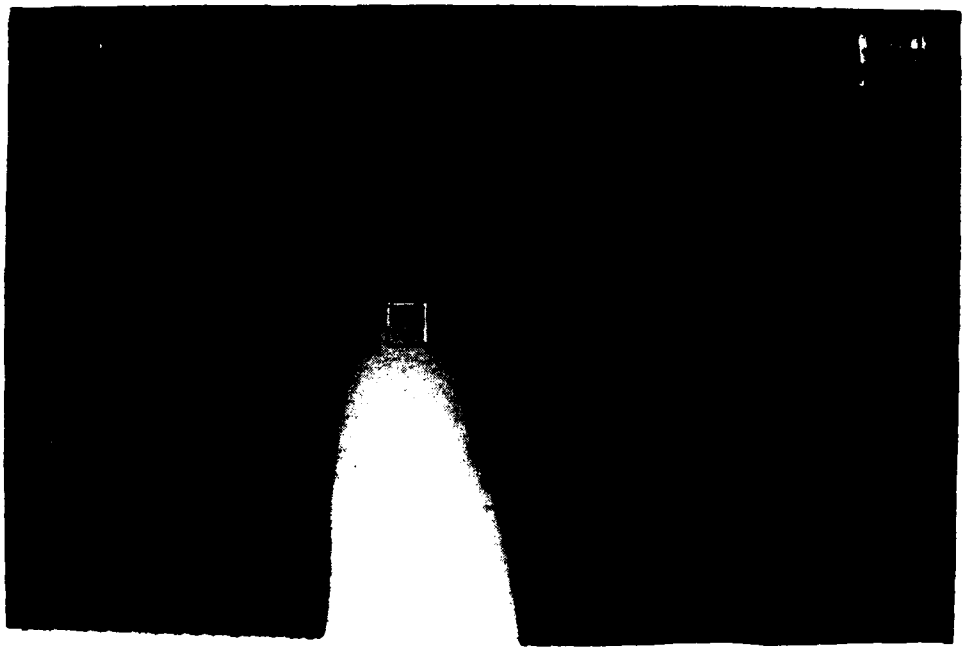

Figure 2.1: Image of bead used to measure temperature.

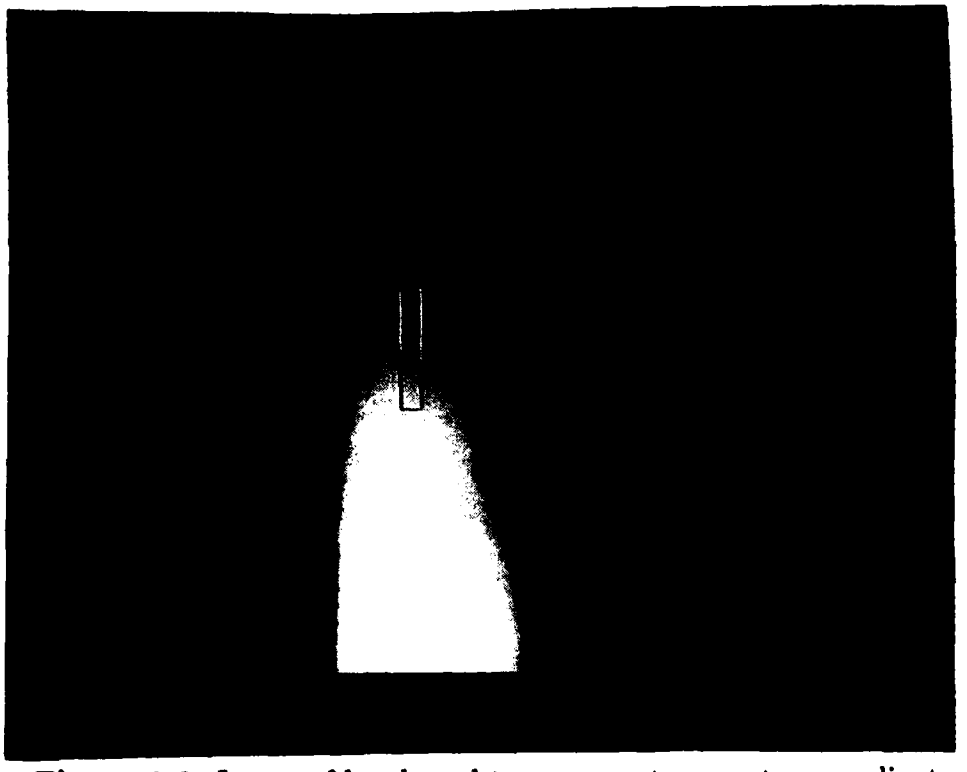

Figure 2.2: Image of bead used to measure temperature gradient.

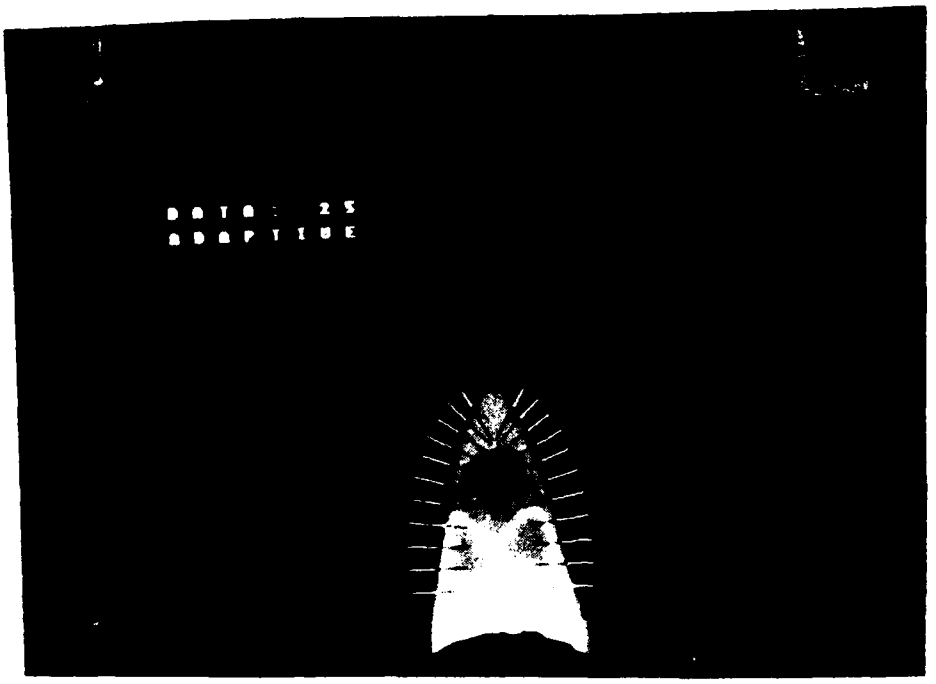

Figure 2.3: Image of weld puddle showing search vectors.

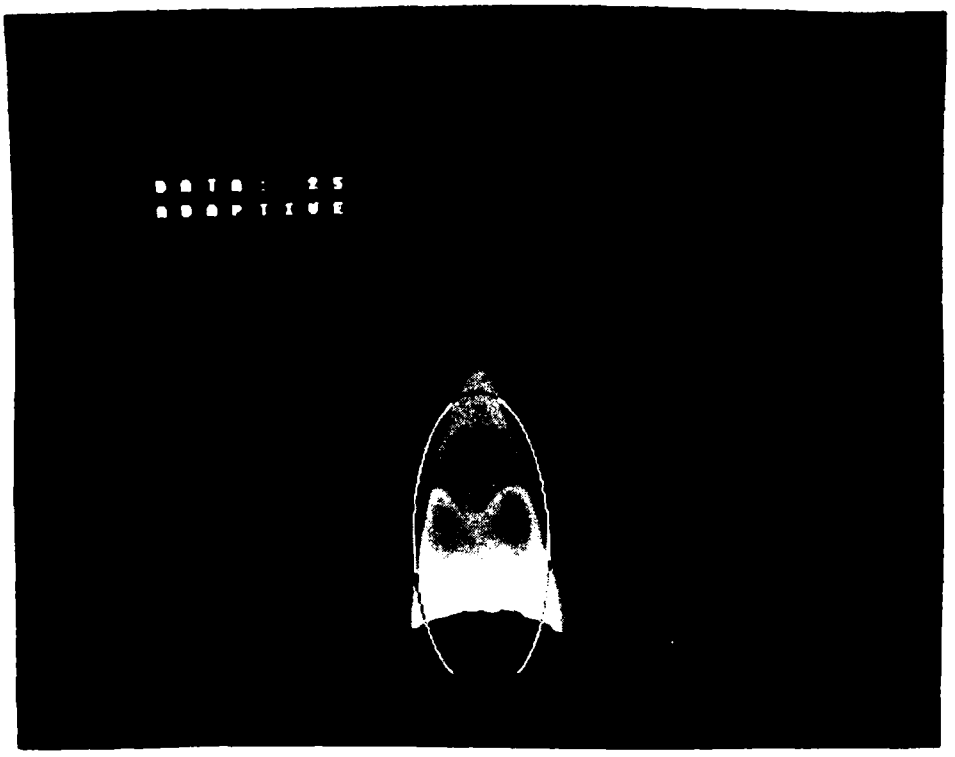

Figure 2.4: Image of weld puddle showing estimated ellipse.

CHAPTER 3

CONTROL SYSTEM STRUCTURE

3.1 Control System Hierarchy

Although it is important to be able to measure all the signals of interest, it is also important to be able to implement a control algorithm. To simplify this task, the control system uses a hierarchical structure. This chapter describes the various control loops and their places in the control system hierarchy as well as some of the standard routines which are available for use by any control algorithm. Since system identification plays a crucial role in the development of a control algorithm, the identification methods available on the system are discussed.

The control system hierarchy adds a great deal of flexibility to the system. This flexibility comes from allowing control of any number of possible system variables. The control loops which have been implemented include travel rate, wirefeed rate, arc current, puddle width and puddle area. In order to control the travel rate and the wirefeed rate, it is necessary to control the voltage applied to the proper motor. However, in order to control the arc current, it is necessary to control the wirefeed rate. Similarly, in order to control the puddle width and puddle area, one must control both the travel rate and the arc current. A method which has been suggested for controlling the cooling rate involves controlling both the puddle width and the puddle area. This hierarchical system allows new control loops to use existing control loops, thus greatly simplifying the task of designing a new control loop.

3.2 Low-Level Loops

The travel rate, wirefeed rate and arc current loops are considered low-level loops since the control of any system variables must include the control of these variables. A block diagram of the low-level system is given in Figure 3.1. All of the low-level loops must have identical sample periods. The normal sample period for the low-level loops is 40 ms. Control laws have already been designed and implemented for sample periods of both 20 ms and 40 ms. The system is designed to allow a low-level sample period of any multiple of 10 ms without changing any software. However, the use of any sample period other than 20 ms or 40 ms will require the design and implementation of a new set of control laws.

The travel rate loop controls the torch velocity in the direction of the weld by applying the appropriate voltage to the travel motor. The control strategy used for this loop is a two-degree-of-freedom polynomial controller. The feedback portion of the controller is designed to give a desired second-order response, and the feedforward portion of the controller is a proportional plus sum (PI) structure.

The wirefeed rate loop uses the voltage to the wirefeed motor to control the rate at which wire is fed to the weld. The control strategy for the wirefeed rate loop is a two-degree-of-freedom polynomial controller, designed to minimize the effects of torque disturbances on the wirefeed rate and to give zero steady-state error in the presence of constant disturbances [17].

The arc current loop uses the wirefeed rate to control the arc current. This places the arc current loop above the wirefeed rate in the control hierarchy since the wirefeed rate is determined by the arc current controller. The control strategy used for the arc current loop is a simple proportional plus sum controller.

3.3 High-Level Loops

The puddle width, puddle area, bead temperature and cooling rate loops are considered high-level loops since any attempt to control these variables must involve the control

of the travel rate, wirefeed rate and arc current. Since the low-level loops are much faster than the high-level loops, it is safe to assume that the dynamics of the low-level loops can be ignored when designing the high-level loops. This allows the high-level loops to be designed with the assumption that the travel rate and arc current are the control inputs. A block diagram of the high-level system is given in Figure 3.2.

The high-level loops which have been implemented include the puddle width and puddle area. The sample period for puddle geometry loops is usually 240 ms. This sample period was chosen to allow the image processing system to perform well. The dynamics of the system would suggest that a slower sample period would be sufficient, but a faster sample period allows the image processing system to track changes in the puddle geometry more closely.

A number of different high-level controllers have been implemented. These include both single input-single output (SISO) and multiple input-multiple output (MIMO) controllers. One high-level controller which has been successfully implemented will be described in detail in Chapter 4. A brief description of other controllers which have been implemented is given here.

One puddle geometry controller implemented on the system was designed by Dan Henderson [18]. This design used the travel rate to control the puddle width. The structure used was an adaptive PI controller based on the method of sensitivity points. This design resulted in a very robust controller which performed well over a wide range of operating conditions.

A second controller was designed by Thierry Bourret [19]. This control design used both arc current and travel rate to control both puddle width and puddle area. The control structure used for this design was a generalized PI. This structure leads to a controller with eight gains. Sensitivity methods were used to adjust these gains off-line in order to decouple the outputs and to follow reference models for each output. Although this design is able to tune itself, the use of many models in the tuning algorithm limits the range of operating conditions with which it can be used.

A third controller was designed by Jeff Schiano [20]. This design used a low-order MIMO model and linear-quadratic (LQ) optimal control techniques to control both the puddle width and the puddle area using arc current and travel rate as inputs. Since no tuning capability was included in the design, this controller is only useful for a limited range of operating conditions.

3.4 Identification Techniques

An important part of the design process is system identification. It is possible with some systems to develop a dynamic model based on physical principles. However, many systems are too complex for this approach to be useful. With these systems, it is necessary to use identification techniques to develop a model. The welding system at USACERL has both an on-line identification scheme and the capability to export data to a separate program for identification or analysis. The program commonly used for this task is $Matrix_x$, since it has many different identification algorithms.

The on-line identification scheme implemented on the system is recursive least squares. This identification scheme is limited to SISO discrete-time systems. Currently, no filtering is done on the data before or during the identification routine. This makes the on-line identification very susceptible to noise problems.

The off-line identification schemes are much more flexible. The routines which have been used with the welding system include recursive least squares, approximate maximum likelihood, recursive maximum likelihood and maximum likelihood [25],[26]. Balanced truncation has also been used been used to reduce the order of the models [27].

The algorithm which has been used most often with the welding system starts with recursive least squares. The model found by this algorithm acts as a starting point for the approximate maximum likelihood algorithm. This model is in turn used as a starting point for the recursive maximum likelihood algorithm. The maximum likelihood techniques are stochastic in nature and attempt to filter the data to minimize the effects

of noise. This results in a much more accurate model than can be found by using recursive least squares alone.

One drawback to the identification method outlined above is that it can only be used for SISO systems. In order to find a MIMO model, maximum likelihood can be used. After identifying SISO models of parts of the system separately, it is possible to combine them into a single MIMO model and to use maximum likelihood to tune the model. This method can also be used with balanced truncation to reduce the order of the SISO models before incorporating them into a MIMO model. This method was used by Schiano to give an accurate low-order MIMO model of the puddle geometry.

All of the techniques for identification which have been mentioned here are available on $Matrix_x$. Since $Matrix_x$ is such a valuable tool for designing and simulating control systems, the welding system has been programmed to be able to read and write data files that are compatible with $Matrix_x$. This greatly simplifies the process of analyzing data and designing a controller for the welding system.

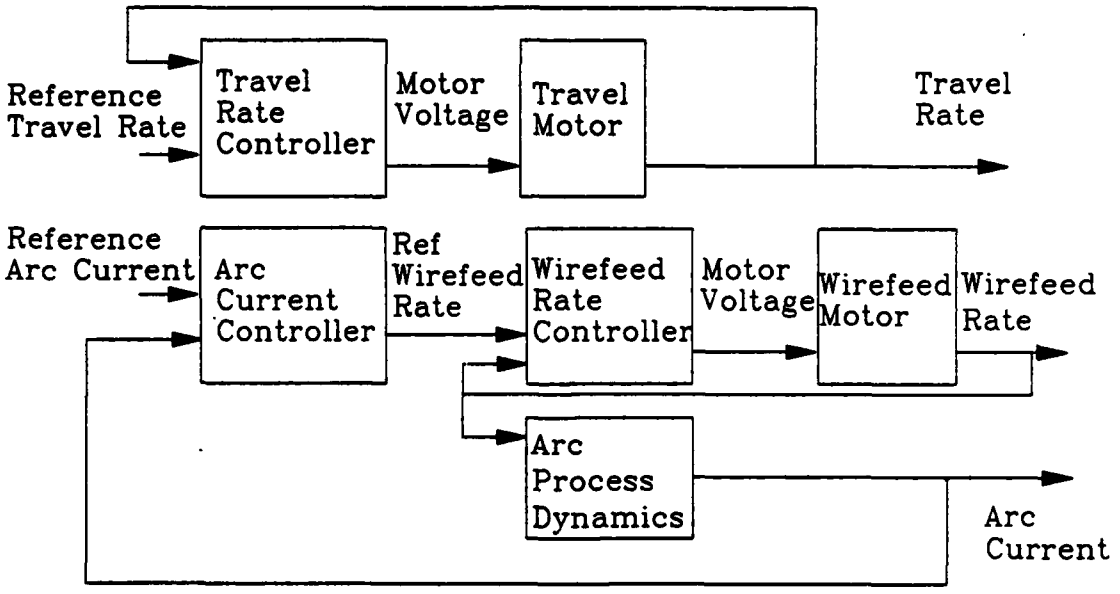

Figure 3.1: Block diagram of low-level system.

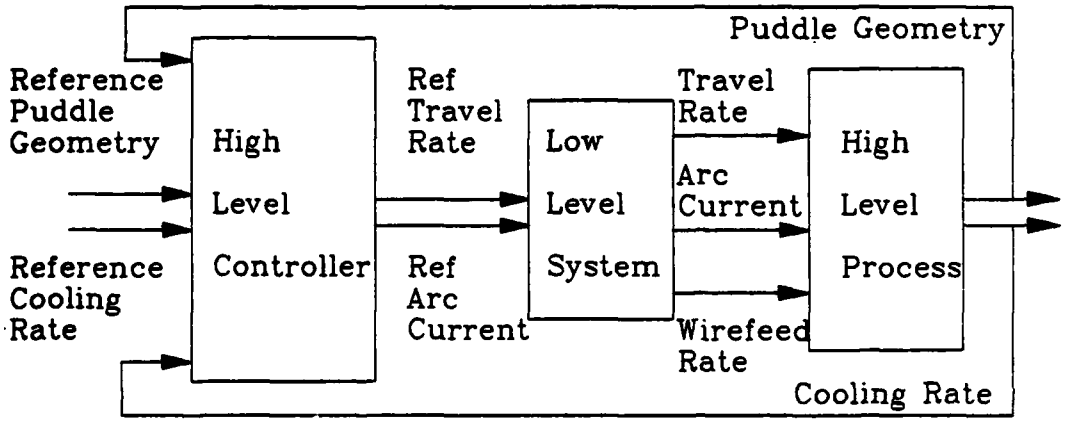

Figure 3.2: Block diagram of high-level system.

CHAPTER 4

A CONTROL SYSTEM EXAMPLE

4.1 Preliminary Experiments

A set of preliminary experiments was conducted to establish an operating envelope, which is centered around a travel rate of 13 IPM and an arc current of 360 A. Acceptable welds are obtained when the travel rate and arc current lie in the ranges of 8 IPM to 18 IPM and 310 A to 410 A, respectively. These experiments also revealed the presence of oscillatory modes in the puddle width and puddle area response. Frequency analysis of data taken at the nominal operating point revealed several peaks near 0.2 Hz. This result is not surprising in light of recent studies on weld puddle oscillations [22]-[24]. These modes are driven in part by the electrode droplets that strike the surface of the weld puddle. The oscillation frequencies are closely related to the mass of the weld puddle and, therefore, depend on the travel rate and arc current.

Since many factors influence the dynamic response of the puddle width, it is important to limit the effects of as many of these factors as possible. The power supply voltage, shield gas composition, and shield gas flow rate are identical for all experiments. In each experiment, a bead is deposited on a 48″ by 16″ by 1″ plate of A36 structural steel. Prior to each experiment, the plate is preheated to 250° F by raising the surface temperature to 300° F and allowing the plate to passively cool. As the plate cools, the thermal energy equilibrates so that the surface temperature along the weld line is uniform to within 15° F before the experiment is started. This procedure was necessary since puddle geometry is affected by the initial plate temperature [21].

4.2 Identification Experiments

Preliminary experiments revealed the presence of highly underdamped modes in the puddle geometry response. The control strategy is to incorporate the oscillatory modes into the model and to design the controller to attenuate the amplitude of the oscillations. This differs from the approaches used to design the controllers discussed previously. The approach used to design the other controllers was to neglect the oscillatory modes and to model the dynamics with a low-order system. In these cases, the bandwidth of the closed-loop system was reduced so as not to excite the oscillatory modes. The model which includes the oscillatory modes will be used to design a linear-quadratic (LQ) controller which regulates only puddle width using travel rate as a controlled input.

One minute of data was collected for identification. In this experiment, the arc current was regulated to 360 A while the travel rate was varied. The time-varying input consists of two superimposed square waves. One component has a 50 sec period and is included to reveal information on the steady-state response to various input levels. The second component has a period of 10 sec and provides good frequency content for exciting the oscillatory modes of the puddle.

The input sequences and the resulting puddle width response are shown in Figure 4.1. Figure 4.1(a) shows the input sequences used for the identification experiment, and Figure 4.2(b) shows the puddle width response. The puddle width plot was obtained by subtracting off the mean puddle width of 0.64 inches. This is necessary before identification since a linear model around the operating point is desired. The puddle width response has a much larger amplitude over the second half of the experiment than it does at the start. Since the identification sequence was designed to excite the oscillatory modes, this is not surprising.

4.3 Single-Input Single-Output Model

A single-input single-output (SISO) model relating travel rate to puddle width is identified in three steps. An initial estimate is obtained using recursive least-squares.

The resulting model is refined by employing recursive maximum likelihood estimation followed by approximate maximum likelihood estimation. These additional steps reduce the effect of noise in the identification process [25], [26]. Models of various orders and relative degrees were found and compared for their ability to capture both the salient response of the puddle width and the puddle resonances. This approach led to the sixth-order model

$$\frac{Y(z)}{U(z)} = \frac{10^{-3}\left(.0912z^5 - .307z^4 - .776z^3 + .0933z^2 - 1.80z - 1.50\right)}{z^6 - .698z^5 - .315z^4 + .123z^3 - .411z^2 + .195z + .215} \tag{4.1}$$

where y_k and u_k are the puddle width and travel rate measured with respect to the nominal operating point

$$\begin{aligned} y_k &= \textit{puddle width} - 0.63\ \textit{in} \\ u_k &= \textit{travel rate} - 13\ IPM \end{aligned}$$

It is convenient to represent this model in state-space form. Since the physical meaning of the states is unknown, any state-space realization may be used. A balanced realization is used due to its superior numeric properties and the additional insight it provides [27]. The balanced realization of the transfer function (4.1) is

$$\begin{aligned} x_{k+1} &= A_m x_k + B_m u_k \\ y_k &= C_m x_k \end{aligned} \tag{4.2}$$

where

$$A_m = \begin{pmatrix} 0.9615 & 0.1413 & -0.0304 & -0.0181 & -0.0173 & -0.0004 \\ -0.1413 & 0.8766 & 0.0112 & 0.0489 & 0.0633 & 0.0019 \\ -0.0304 & -0.0112 & 0.2660 & -0.7848 & 0.0049 & 0.0106 \\ 0.0181 & 0.0489 & 0.7848 & -0.0226 & -0.3912 & -0.0146 \\ -0.0173 & -0.0633 & 0.0049 & 0.3912 & -0.6785 & 0.0249 \\ -0.0004 & -0.0019 & 0.0106 & 0.0146 & 0.0249 & -0.0001 \end{pmatrix}$$

$$B_m = \begin{pmatrix} 0.0479 & 0.0559 & 0.0266 & -0.0141 & 0.0152 & 0.0004 \end{pmatrix}^T$$

$$C_m = \begin{pmatrix} -0.0479 & 0.0559 & -0.0266 & -0.0141 & -0.0152 & -0.0004 \end{pmatrix}$$

The sixth-order SISO model relating travel rate to puddle width captures the oscillatory behavior of the puddle width. This model is used in Section 4.4 to design a controller for the puddle width.

4.4 Linear Quadratic Control

Optimal LQ control methods [27],[28] and sensitivity point tuning [29], [30] are used to design a puddle width controller that rejects constant disturbances and that reduces the amplitude of oscillation in the frequency range 0.1 Hz to 0.4 Hz without reducing the bandwidth of the system. Constant disturbances are rejected by appending an accumulator state to the system model. The accumulator state must be included in the output so that the resulting system (A, B, C) is observable

$$A = \begin{pmatrix} A_m & 0 \\ T_s C_m & I \end{pmatrix} \quad B = \begin{pmatrix} B_m \\ 0 \end{pmatrix} \quad C = \begin{pmatrix} C_m & 0 \\ 0 & 1 \end{pmatrix} \tag{4.3}$$

where the sample time T_s is 240 ms. Sensitivity point tuning is used to improve the response in the frequency range of interest.

The feedback law

$$u_k = -K_R \hat{x}_k \tag{4.4}$$

is implemented with K_R chosen to minimize the cost functional

$$J_R = \sum_{k=0}^{\infty} [x_k^T R_{xx} x_k + u_k^T R_{uu} u_k] \tag{4.5}$$

where R_{xx} and R_{uu} are weighting matrices and $\hat{x}_k$ is an estimation of the state x_k.

The selection of an appropriate weighting matrix is simplified since the SISO model (A_m, B_m, C_m) is in balanced realization form. The diagonal elements of the weighting matrix should reflect the fact that the states are arranged in decreasing order of significance. It is important to note that the accumulator state was appended after finding a balanced realization. This means that the first six states are in decreasing order of significance, and the seventh state is simply placed in the last position for convenience.

By alternately modifying the weighting matrices and simulating the closed-loop response the following set of matrices was chosen:

$$\begin{aligned} R_{xx} &= diag\,(1000, 1000, 100, 100, 10, 10, 10000) \\ R_{uu} &= 1 \end{aligned} \tag{4.6}$$

The state estimator is given by

$$\hat{x}_{k+1} = A\hat{x}_k + Bu_k + K_E(y_k - C\hat{x}_k) \tag{4.7}$$

where the estimator gain K_E is chosen to minimize the cost functional

$$J_E = \sum_{k=0}^{\infty} [x_k^T Q_{xx} x_k + y_k^T Q_{yy} y_k] \tag{4.8}$$

where Q_{xx} and Q_{yy} are the state and output noise covariance matrices, respectively.

The covariance matrices are calculated from experimental data collected during a 180 sec interval in which the travel rate and arc current are regulated to 13 IPM and 360 A, respectively. The rms value of the input u_k is calculated from the travel tachometer and used to construct the state covariance matrix

$$Q_{xx} = B\,(rms\ value\ of\ u_k)\,B^T \tag{4.9}$$

The output covariance matrix is diagonal and is formed using measurements of the puddle width. The diagonal elements are the rms values of the two components of y_k, respectively.

The performance of the regulator was improved further by adjusting the regulator and estimator gains to attenuate the puddle width oscillations. The gains were adjusted directly since it was not obvious how to choose the weighting matrices to reduce the amplitude of oscillations. On the other hand, the method of sensitivity tuning provides a means to achieve this goal. The change in the puddle width response, resulting from a change in a gain, is described by a sensitivity function, which for a given gain can be generated from computer simulations. Since the sensitivity function shows how changes in a gain affect the puddle width response, the gain can be adjusted to improve the response.

The regulator and estimator gains were updated several times using this method to reduce the puddle width response in the frequency range 0.1 Hz to 0.4 Hz.

The final tuned gains used for the closed-loop experiments are

$$K_R = \begin{pmatrix} 27.129 & 3.999 & .087 & .492 & .244 & .087 & -109.990 \end{pmatrix}^T \tag{4.10}$$

$$K_E = \begin{pmatrix} -7.635 & .545 & .003 & -.014 & -.011 & -.002 & .085 \\ -0.211 & .318 & -.031 & -.005 & -.011 & -.001 & .123 \end{pmatrix}^T$$

The gains corresponding to the first states are larger because the SISO model (A_m, B_m, C_m) is in balanced realization form. It is obvious that the seventh state, which is the appended accumulator state, has the largest influence on the output. This is easy to understand since the output was redefined to include the accumulator state as an extra output. Although these gains are no longer optimal for the original weighting matrices and noise covariance matrices, it is easy to see that a set of cost functionals can be defined for which these gains are optimal. This approach is advantageous since the sensitivity method leads to a desired response in a small number of iterative steps.

Figure 4.2 shows the results for the control experiments. The arc current in each experiment was regulated to 360 A. Figure 4.2(a) shows the open-loop puddle width response for a travel rate of 13 IPM. The average puddle width is 0.57″ and the peak-to-peak amplitude of the oscillations is approximately 0.05″. Figure 4.2(b) shows the response of the closed-loop system for a puddle width command of 0.57″. This command was chosen so that the operating point for the two experiments is the same. The data in Figure 4.2(b) show that the controller is capable of regulating the puddle width to the desired value. Frequency analysis of the data in Figures 4.2(a) and 4.2(b) shows that components in the 0.1 Hz to 0.4 Hz range are 3 dB to 6 dB smaller for the closed-loop system. On the other hand, in comparison to the open-loop response, the closed-loop system accentuates frequency components above 0.4 Hz. In Figure 4.2(c) the operating point was shifted by requesting a puddle width of 0.49″. The resulting travel rate command was about 16 IPM. In this case, the amplitude of the puddle oscillations was increased both inside and outside the 0.1 Hz to 0.4 Hz frequency range.

4.5 Results

The control strategy incorporated the oscillatory behavior of the puddle into the system model, and the controller was designed to reduce the amplitude of these oscillations. The controller achieved only a slight improvement in performance by reducing the amplitude of the puddle oscillations by several decibels in the frequency range of interest. However, above 0.4 Hz, the amplitude of the puddle oscillations was increased by several decibels. This suggests that concentrating on reducing the oscillations within a certain range of frequencies can cause problems in other frequency ranges. This phenomenon has also been noticed on other systems. The Hubble spacecraft had a low-frequency oscillation problem which, when corrected, became an oscillation problem at a higher frequency [31]. A more reasonable design goal would be to let the system oscillate at its natural frequency and simply reduce the bandwidth of the system so that those modes are not excited.

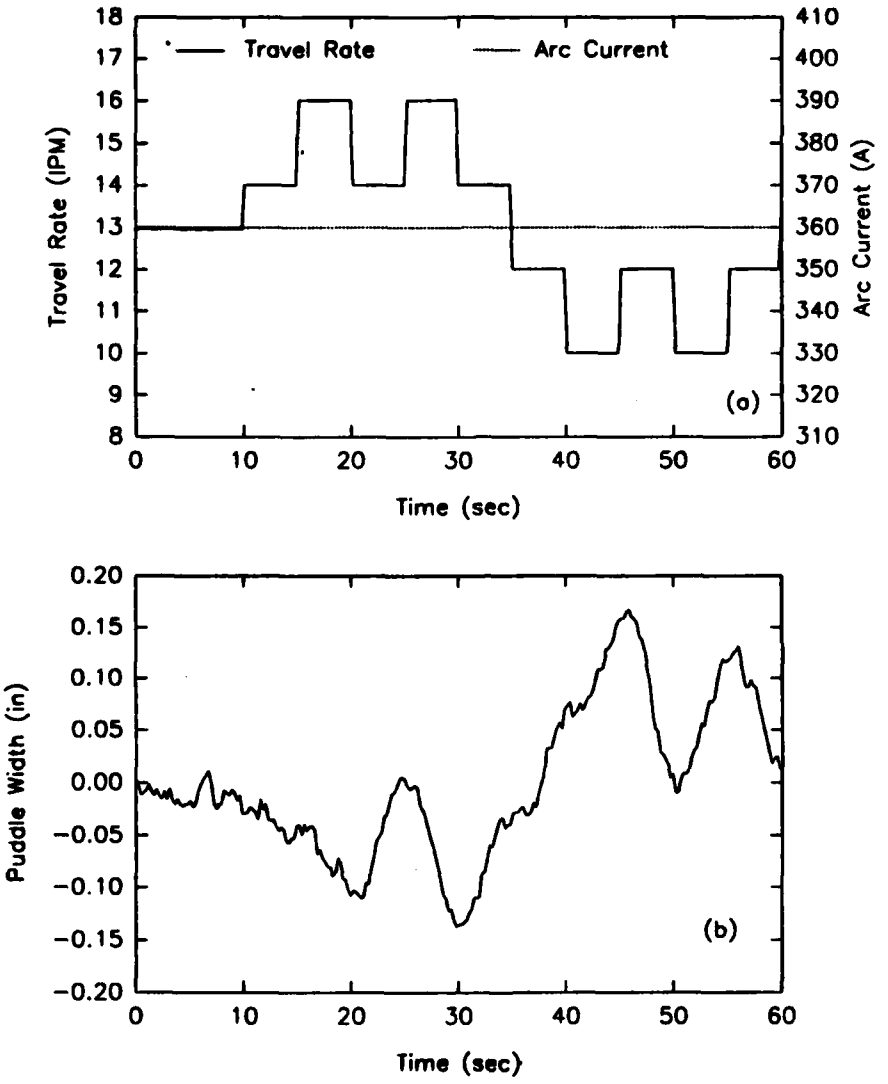

Figure 4.1: (a) Input sequences for identification experiment. (b) Puddle width response to variation in travel rate.

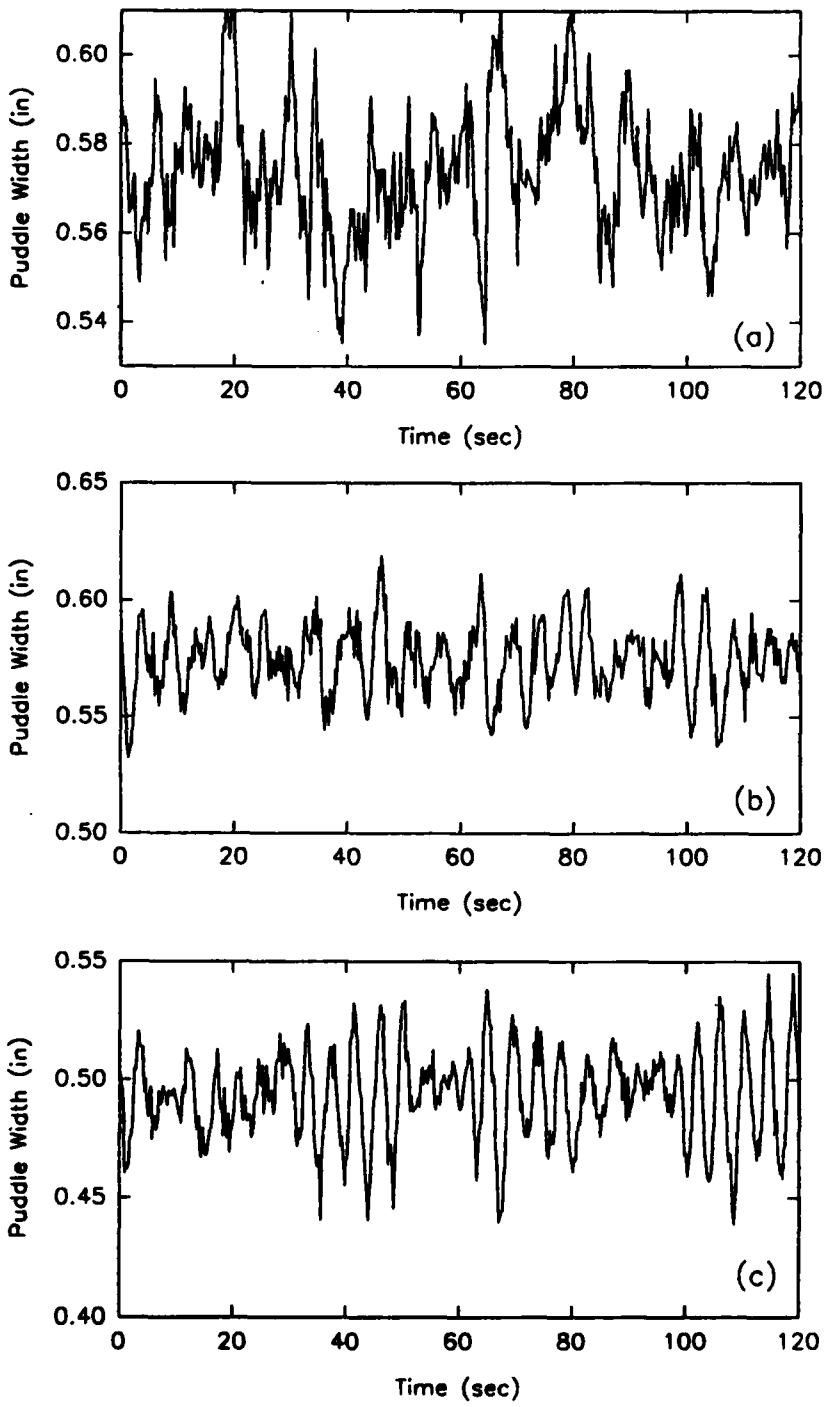

Figure 4.2: (a) Open-loop puddle width for a travel rate of 13 IPM. (b) Closed-loop puddle width at same operating point. (c) Closed-loop puddle width at different operating point.

CHAPTER 5

DISCUSSION AND SUMMARY

The automated welding system has many capabilities. One of these capabilities is to enable state of the art research to be done. Another capability of the system is to enable new or even old control theories to be implemented easily and tested against other algorithms.

The ability to do research on this system is obvious. Many new methods of measuring and controlling variables in the welding process have already been implemented. The possibility to continue doing this is present. Control laws have been developed which decouple the puddle width and puddle area. A control law has been implemented which regulates the puddle width and adapts to new or changing conditions in real time. The next step is to develop an adaptive algorithm for regulating both puddle width and puddle area. The cooling rate is a very important parameter in the quality of a weld. At this time, the new method of measuring the cooling rate has not been used in a closed-loop system. The puddle oscillations seen in Chapter 4 may contain information about the quality of the weld. The image processing system works fairly well, but perhaps a different approach could provide more information. This short list of ideas represents many possible research topics which remain to be explored.

The welding system's ability to be used as a testbed for implementing control algorithms could be extremely useful. New control theories could be tested for practicality. Implementing any control algorithm is a very useful learning process. Although much of the work involved with implementing a system has already been completed, the potential

for learning has not been diminished. Both graduate and undergraduate students could benefit from using an actual system rather than of running simulations.

All of the work which went into designing the system has been documented. Many papers and theses have been written about this work [16]-[20],[32]. These papers contain information about the type of work which has been done with the welding system. In addition, those who wish to use the system can find complete documentation available at USACERL. The software documentation includes a user's guide and a programmer's guide to both the control code and the image processing code. In addition, a beginner's manual has been written which leads the new user through the steps necessary to use the system software. The hardware documentation includes circuit schematics, pin layouts and connection diagrams for all of the hardware.

Anyone interested in further information about the welding system can contact one of the following people at USACERL. Robert Weber is the head of the Welding Technology Center at USACERL. He can be reached by calling 352-6511 and asking for extension 239. His mailing address is Robert Weber, EM-MQA, USACERL, P. O. Box 4005, Champaign, IL 61824-4005. Will Windes is familiar with the welding system and can be reached by calling 352-6511 x477. Jim Ross can be reached by calling 352-6511 x334. Jeff Schiano can be reached on the University of Illinois campus by calling 333-7469. These phone numbers are current at this time and may soon be out of date. However, it should be possible to get information by calling USACERL and asking to talk to someone in the EM-MQA Team.

APPENDIX

IMAGE PROCESSING DEVELOPMENT

A number of different algorithms have been used to measure puddle width and puddle area. This Appendix is an attempt to document the algorithms which have been used. Many of the algorithms were simple variations of others which were attempted. However, for a number of reasons some algorithms were more successful than others. The algorithm described in Chapter 2 was the most successful. The algorithms described in this Appendix are given so that attempts to improve the image processing system do not repeat methods previously used.

Two main algorithms have been used to estimate an ellipse given the boundary data. The first algorithm used was developed using matrix manipulations and was based on the least-squares algorithm given by Leon [33]. This algorithm was very susceptible to noise problems. By contrast, the algorithm developed by Baheti which is currently being used is very robust with respect to noisy data [8].

Baheti's algorithm is developed under the following assumptions. First, the approximate size and location of the weld puddle are known in advance. Second, the location of one focus of the ellipse must be known. Third, this focus is located at the position of the electrode. Once Baheti's algorithm was implemented, it became clear that some of the assumptions listed above are not always valid. In particular, fixing the location of the focus of the ellipse at the electrode center seemed to cause the algorithm to have problems. An algorithm was developed to estimate four parameters instead of just two. The two extra parameters corresponded to the location of the focus. However, the extra degrees of freedom associated with these parameters allowed the algorithm to fit a hy-

perbola or a parabola to the data instead of an ellipse. It was quickly apparent that this was not the solution. The next approach that was attempted involved fixing the location of the electrode center along the weld line and estimating the center of the electrode in the other direction. Once this parameter is determined, Baheti's algorithm can be used. This approach gave another degree of freedom while retaining the desirable properties of Baheti's algorithm and resulted in greatly improved estimation of the puddle width and area.

After implementing the estimation routine for the electrode center and the ellipse, it was necessary to improve the method used to find points on the boundary of the weld puddle. The search vectors that are used to find the boundary data are explained in Chapter 2. The first method used to find the boundary data compared the pixel grey level of the search vectors to a predetermined threshold level. This method was ineffective since the grey level of the image is much higher near the arc than it is near the tip of the weld puddle. This means that no one threshold grey level can be used to find the boundary at every region of the image.

Next, several methods were developed and tested for finding the boundary along each search vector. One method is to find the maximum grey level difference between adjacent groups of pixels. This average gradient method was not effective since the noise level is much higher than that for the actual gradient of the boundary in many regions of the weld puddle. Another disadvantage to this method is that it is numerically intensive. A third method was developed using a statistical approach. The mean and variance of the pixel grey levels were calculated for each search vector. Using the mean value of the grey level for each search vector as a threshold for that search vector resulted in boundary data that were very close to those for the actual boundary. By considering search vectors of varying lengths, it was discovered that averaging along the entire length of the search vector could result in a biased estimate. This effect can be minimized by averaging only the pixels at each end of the search vector in order to determine a threshold level for that search vector. This approach has two advantages. First, the boundary points found by this method are very close to the actual boundary of the weld puddle. Second,

this approach is very simple to implement and is not appreciably slower for long search vectors.

The width and area of the weld puddle vary over a wide range of shapes and sizes. The search vectors must be able to detect the boundary points regardless of the location of the boundary. One method which would make this possible would be to use long search vectors; however, this has proven in practice to give noisy measurements. Another solution is to use short search vectors and to locate these search vectors near the puddle boundary. Originally, the pixel locations of one set of search vectors were determined at the start of a weld and used for each image. By finding the pixel locations of a new set of search vectors for each image, tracking the changing size and shape of the weld puddle becomes much easier. In this way, the image processing system becomes dynamic.

Other parameters which can be changed include the number of search vectors and the included angle of the search vectors. The number of search vectors can vary from three to fifty. The current algorithm uses twenty-one search vectors. Adding more search vectors provides more information at the expense of greatly increased processing time. The included angle of the search vector is measured from the vertical direction. If the initial angle is 0°, there will be a vertical search vector. An angle of 90° or greater corresponds to a horizontal search vector. Any angle greater than 90° will simply move the horizontal search vector closer to the electrode center.

REFERENCES

[1] R. D. Stout, *Weldability of Steels.* New York: Welding Research Council, 1987.

[2] *Welding Handbook*, American Welding Society, Vols. 1, 4, 8th ed., 1987.

[3] N. D. Malmuth, W. F. Hall, B. I. Davis and C. D. Rosen, "Transient Thermal Phenomena and Weld Geometry in GTAW," *Welding Journal*, Research Suppl., vol. 53, no. 9, pp. 388s-400s, 1974.

[4] A. R. Vroman and H. Brandt, "Feedback Control of GTA Welding Using Puddle Width Measurements," *Welding Journal*, vol. 55, no. 9, pp. 742-749, 1976.

[5] R. W. Richardson, D. A. Gutow and S. H. Rao, "A Vision Based System for Arc Weld Pool Size Control," *Measurement and Control for Batch Manufacturing*, D. E. Hardt *Ed.*, *ASME*, NY, pp. 65-75, 1982.

[6] R. W. Richardson, D. A. Gutow, R. A. Anderson and D. F. Farson, "Coaxial Arc Weld Pool Viewing for Process Monitoring and Control," *Welding Journal*, vol. 63, no. 3, pp. 43-50, 1984.

[7] N. R. Corby, "Machine Vision Algorithms for Vision Guided Robotic Welding," *Proceedings of the* 4th *International Conference on Robot Vision and Sensory Controls*, London, pp. 137-147, 1984.

[8] R. S. Baheti, "Vision Processing and Control of Robotic Arc Welding System," *Proceedings of* 24th *Conference on Decision and Control*, Ft. Lauderdale, FL, pp. 1022-1024, 1985.

[9] E. A. Gladkov, "An Automatic Stabiliser of Penetration in Plasma Welding with a Penetrating Arc," *Welding Production*, no. 11, pp. 26-27, 1977.

[10] P. Boughton, G. Rider and C. J. Smith, "Feedback Control of Weld Penetration in 1978," *Advances in Welding Processes*, The Welding Institute, pp. 203-215, 1978.

[11] H. Nomura, Y. Satoh, K. Tohno, Y. Satoh and M. Kurotori, "Arc Light Intensity Controls Current in SA Welding System," *Welding and Metal Fabrication*, no. 9, pp. 457-465, 1980.

[12] J. J. Hunter, G. W. Bryce and J. Doherty, "On-Line Control of the Arc Welding Process," *Developments in Mechanised, Automated and Robotic Welding*, The Welding Institute, pp. P37-1 - P37-12, 1980.

[13] D. A. Dornfield, M. Tomizuka and G. Langari, "Modeling and Adaptive Control of Arc Welding Processes," *Measurement and Control for Batch Manufacturing*, D. E. Hardt *Ed.*, *ASME*, New York, pp. 53-64, 1982.

[14] D. E. Hardt, D. A. Garlow and J. B. Weinert, "A Model of Full Penetration Arc-Welding for Control System Design," *ASME Journal of Dynamics, Systems, Measurement and Control*, vol. 107, pp. 40-46, 1985.

[15] A. Suzuki and D. Hardt, "Application of Adaptive Control to In-Process Weld Geometry Control," *Proceedings of the 1987 American Control Conference*, Minneapolis, MN, pp. 723-728, 1987.

[16] J. L. Schiano, J. H. Ross, D. E. Henderson and R. A. Weber, "Image Analysis of Puddle Geometry and Cooling Rate in Gas Metal-Arc Welding Process Control," International Society for Optical Engineering, Midwest Technical Conference, September 1990.

[17] B. W. Greene, "Arc Current Control of a Robotic Welding System: Modeling and Control System Design," Report DC-114, University of Illinois, Urbana, IL, 1989.

[18] D. E. Henderson, "Adaptive Control of an Arc Welding Process," Report DC-119, University of Illinois, Urbana, IL, 1990.

[19] T. Bourret, "Off-line Sensitivity Tuning: An Arc Welding Application," Report DC-122, University of Illinois, Urbana, IL, 1990.

[20] J. L. Schiano, "Feedback Control of Two Physical Processes: Design and Experiments," Report DC-00, University of Illinois, Urbana, IL, 1991.

[21] C. M. Adams, "Cooling Rates and Peak Temperatures in Fusion Welding," *Welding Journal*, vol. 37, no. 5, Research Suppl., pp. 210s-215s, 1958.

[22] R. W. Richardson and H. K. Ludewig, "The Effect of Weld Parameter Variations on Pool Oscillations in Full-Penetration Welds," EWI Research Report MR8901, January 1989.

[23] Y. H. Xiao and G. den Ouden, "A Study of GTA Weld Pool Oscillation," *Welding Journal*, Research Suppl., vol. 69, no. 8, pp. 289s-293s, 1990.

[24] R. T. Choo, J. Szekely and R. C. Westhoff, "Modeling of High-Current Arc with Emphasis on Free Surface Phenomena in the Weld Pool," *Welding Journal*, Research Suppl., vol. 69, no. 9, pp. 346s-361s, 1990.

[25] P. R. Kumar and P. Varaiya, *Stochastic Systems: Estimation, Identification and Control.* Englewood Cliffs, NJ: Prentice-Hall, Inc., 1986.

[26] L. Ljung, *System Identification: Theory for the User.* Englewood Cliffs, NJ: Prentice-Hall, Inc., 1987.

[27] R. H. Middleton and G. C. Goodwin, *Digital Control and Estimation: A Unified Approach.* Englewood Cliffs, NJ: Prentice-Hall, Inc., 1990.

[28] B. D. O. Anderson and J. B. Moore, *Optimal Control – Linear Quadratic Methods.* Englewood Cliffs, NJ: Prentice-Hall, Inc., 1990.

[29] P. V. Kokotovic, "The Sensitivity Point Method in the Investigation and Optimization of Linear Control Systems," *System Sensitivity Analysis*, J. B. Cruz, Jr., Ed. Stroudsberg, PA: Dowden, Hutchinson, and Ross Inc., 1973.

[30] P. M. Frank, *Introduction to Sensitivity Theory.* New York, NY: Academic Press, 1973.

[31] "Hubble still shaking despite software 'fix'," *Science News*, vol. 138, no. 19, p. 295, 1990.

[32] J. L. Schiano, J. H. Ross, and R. A. Weber, "Modeling and Control of Puddle Geometry In Gas Metal-Arc Welding," to be presented at the American Control Conference, June 1991.

[33] S. J. Leon, *Linear Algebra with Applications*, 2^{nd} ed. New York, NY: Macmillan Publishing Co., 1986.